Study of νd charged-current two-pion production in the threshold region

D. Day, R. Ammar, D. Coppage, R. Davis, N. Kwak, and R. Stump
University of Kansas, Lawrence, Kansas 66045

S. J. Barish,[a] A. Engler, R. W. Kraemer, K. Miller,[b] and B. J. Stacey[c]
Carnegie-Mellon University, Pittsburgh, Pennsylvania 15213

M. Derrick, T. Dombeck,[d] E. Fernandez,[e] L. Hyman,[f] G. Levman,[g] D. Koetke,[h] B. Musgrave, P. Schreiner,[f] R. Singer,[f] A. Snyder,[i] and S. Toaff[j]
Argonne National Laboratory, Argonne, Illinois 60439

V. E. Barnes, D. D. Carmony, A. F. Garfinkel, and G. M. Radecky[k]
Purdue University, W. Lafayette, Indiana 47907

(Received 13 June 1983)

We present our final results on double-pion production by muon-type neutrinos observed in a 2.4×10^6 (365 000) picture exposure of the Argonne 12-foot deuterium- (hydrogen-) filled bubble chamber. The reactions $\nu d\to\mu^-\pi^-\pi^+pp_s$, $\nu d\to\mu^-\pi^+\pi^0pn_s$, and $\nu d\to\mu^-\pi^+\pi^+nn_s$ are studied. The data, which shows strong $\Delta(1236)$ production, has nucleon-π-π mass distribution peaked at low masses in all three reactions. The excitation functions for the three reactions exhibit a rapid rise over the energy range from threshold up to about 3 GeV, but thereafter the energy dependence appears less pronounced. The threshold behavior of the cross sections for these reactions is analyzed in the context of a model developed by Adjei, Dicus, and Teplitz. Data from the constrained reaction, $\nu d\to\mu^-\pi^-\pi^+pp_s$, satisfy the Adler conserved-vector-current test.

I. INTRODUCTION

While the physics of quasielastic scattering and single-pion production by the weak charged current has been widely studied, both experimentally and theoretically,[1-6] very little data exist for the exclusive reactions involving two or more pions.[3,7] In this paper, we present our final results on two-pion production from ν_μ interactions in the Argonne 12-foot bubble chamber. The exposures comprise 2.4×10^6 and 365 000 pictures taken with a deuterium and hydrogen filling, respectively, corresponding to a total of 5.8×10^{18} protons on target at a momentum of 12.4 GeV/c. The hydrogen film represented 13% of the total film but accounted for only 5% of the data because of lower neutrino intensity during the hydrogen run.

The reactions studied are $\nu d\to\mu^-\pi^-\pi^+pp_s$, $\nu p(n_s)\to\mu^-\pi^+\pi^0p(n_s)$, and $\nu p(n_s)\to\mu^-\pi^+\pi^+n(n_s)$. The neutrino energy spectrum at the Zero Gradient Synchrotron peaks at 0.5 GeV and falls off rapidly at higher energies, providing data up to an energy of 6 GeV for events in the sample.[3] This experiment is therefore well suited to study the threshold behavior of two-pion production. Details of the experimental arrangement, and of the scanning and measuring procedures, have been given previously.[1]

II. EVENT SELECTION

Events representing the reactions

$$\nu d\to\mu^-\pi^-\pi^+pp_s\ , \tag{1}$$

$$\nu d\to\mu^-\pi^+\pi^0pn_s \text{ or } \nu p\to\mu^-\pi^+\pi^0p\ , \tag{2}$$

$$\nu d\to\mu^-\pi^+\pi^+nn_s \text{ or } \nu p\to\mu^-\pi^+\pi^+n \tag{3}$$

were obtained by scanning for interactions having three, four, or five tracks. The film was partially double- and triple-scanned; the correction factors for the scanning and measuring inefficiencies are given in Table I.

Reaction (1) is well constrained, and its kinematic identification poses little problem. However, both reactions (2) and (3) are kinematically underconstrained and are also difficult to separate because of their similarities. When the spectator nucleon was unseen, we employed the stan-

TABLE I. Summary of rate corrections.

(a) Reaction (1)	
Scanning efficiency	1.00±0.01
(b) All reactions	
Measuring efficiency	1.09±0.02
Missing low q^2	1.10±0.09
(c) Reactions (2) and (3)	
Scanning efficiency	1.07±0.02
Neutrino single-pion loss	1.09±0.03
Spectator cut	1.11±0.04
Loss of underconstrained events	1.05±0.01
Correction for $\theta_{\mu^-h^+}>150°$	1.06±0.01
(d) Reaction (3)	
Correction for $\theta_{\nu n}$	1.11±0.09

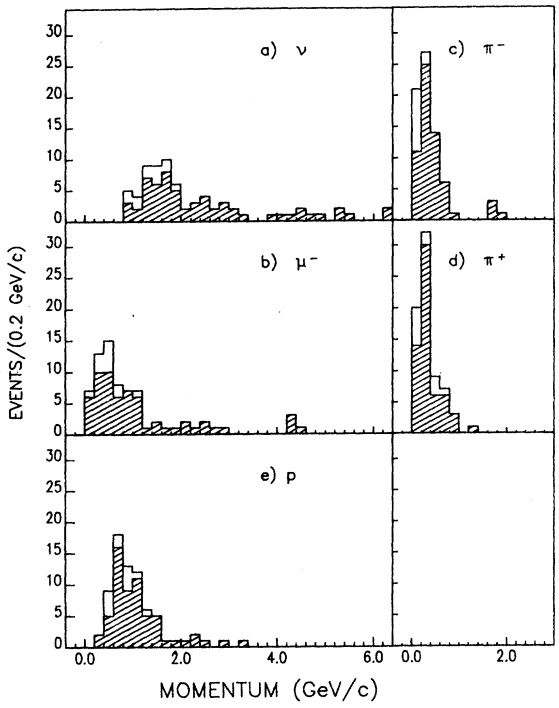

FIG. 1. Momentum distributions for reaction (1). The cross-hatched areas are unique events, while the blank areas are events with $M(\pi^- p) = M(\Lambda) \pm 15$ MeV/c^2.

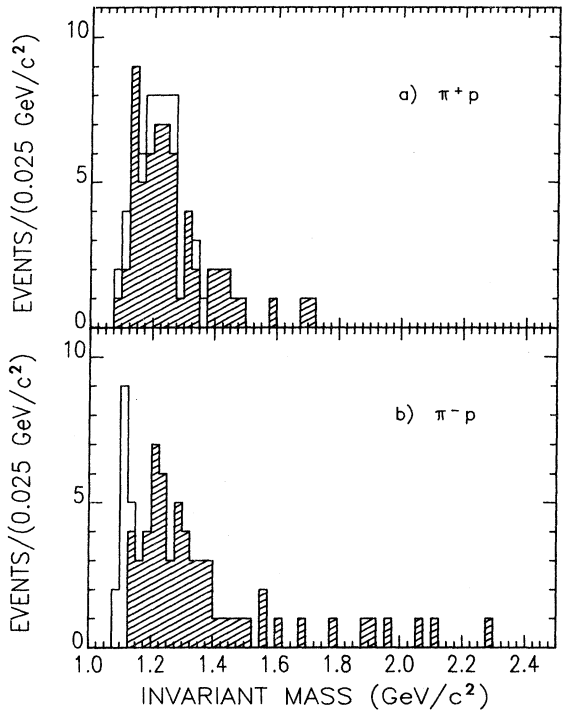

FIG. 2. The pion-nucleon invariant-mass distributions for reaction (1). The cross-hatched areas are unique events, while the blank areas are events with $M(\pi^- p) = M(\Lambda) \pm 15$ MeV/c^2. For (a), the low-mass peak is a reflection of the Δ^0. For (b), the Δ^{++} reflection lies just above the Δ^0 peak.

dard procedure of using the starting values $p_x = p_y = p_z = 0 \pm 50$ MeV/c in the kinematic fit. For reactions (2) and (3) this procedure results in a loss of events with high spectator momentum. Corrections for this loss were made by comparing the observed and expected spectator-momentum distributions[5] and are given in Table I.

A. The reaction $\nu d \to \mu^- \pi^- \pi^+ p p_s$

The data sample consisted of those four- and five-prong events which satisfied the following criteria: (a) there was a three-constraint (3C) or two-constraint (2C) fit to reaction (1) with χ^2 probability greater than 1%, (b) the results of the fit were consistent with the visual information (ionization, scattering, stopping tracks, γ conversions, etc.) on the film, (c) one of the negative tracks was consistent with being a muon, i.e., it either left the bubble chamber without interacting or gave an observed $\mu^- \to e^-$ decay, and (d) the interaction occurred within a specified fiducial volume which varied from 9 to 11 m^3 depending on the run. These criteria yielded 73 events of which 38 had a unique muon-track assignment with the remaining 35 events having two tracks that were μ^- candidates. In addition, 7 of the 73 events had a π^+/p ambiguity for the positive tracks.

For the 35 events having the muon-track ambiguity, the higher-momentum noninteracting negative track was chosen to be the muon. With this assignment the resulting π^- and π^+ momentum distributions are then very similar, as shown in Figs. 1(c) and 1(d). In addition, the μ^- momentum spectrum resembles the μ^- spectra in reactions (2) and (3) where there is no negative-track ambiguity. A possible bias favoring low momentum transfer may be expected as a result of this procedure.

For the 7 events where a π^+/p ambiguity remained, the higher-momentum track was chosen as the proton. The justification for this lies in the observation that the proton had a higher momentum than the pion in 92% of the unique fits to reaction (1) when at least one of the positive tracks had $p > 0.55$ GeV/c.

Finally, because of the relatively poor spatial resolution of this bubble chamber it is possible that the data sample is contaminated by events containing a Λ which decays close to the production vertex. The $\pi^- p$ effective-mass distribution shown in Fig. 2(b) does in fact show an excess of events in the region of $\Lambda(1115)$. From this distribution we estimate that 6 events are Λ^0 decays where the separation of vertices is not seen, consistent with the number predicted from the decay distribution for events where the decay vertex is observed. The final sample for reaction (1) therefore contains 67 events.

B. The $\mu^- \pi^+ p \pi^0$ and $\mu^- \pi^+ \pi^+ n$ final states in hydrogen and deuterium

As discussed previously, the assignment of events to these final states is more difficult than for the constrained

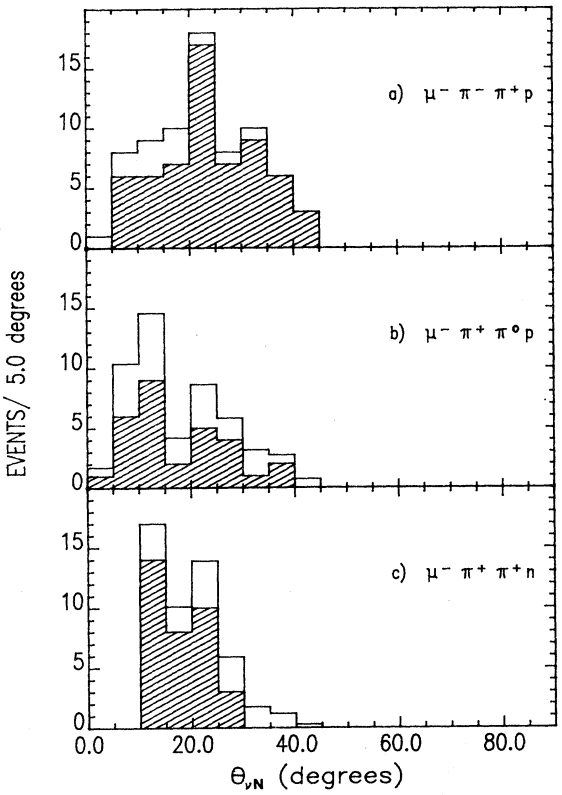

FIG. 3. Distributions of $\theta_{\nu N}$, the angle between the neutrino direction and the nonspectator nucleon. The cross-hatched areas in (a) are unique events, while the blank areas are events with $M(\pi^- p)=M(\Lambda)\pm 15$ MeV/c^2. In (b) and (c) the cross-hatched areas are the uniquely chosen events for the reaction. The blank areas are the ambiguous events weighted as discussed in the text. In (c), the events with $\theta_{\nu N}$ less than 10° were deleted.

reaction (1). The raw data sample consisted of all three-prong events that gave a 0C solution to either reaction (2) or (3). For those events with one or more associated γ conversions or a secondary neutron interaction, this information was included, when possible, in the kinematic fit. There were three such events for reaction (2) and two for reaction (3).

The raw sample was then subjected to a number of cuts to reduce the background due to spurious fits. At our energies, quasielastic scattering and single-pion production are much more likely than double-pion production. We therefore discarded those events fitting the 3C or 2C reac-

TABLE II. 0C ambiguity-resolution parameters.

Momentum range (GeV/c)	Unique events: Proton from reaction (2)	Unique events: Fast pion from reaction (3)	Ambiguous events
0.00–0.55	11	13	1
0.55–1.00	11	19	13
>1.00	8	3	23

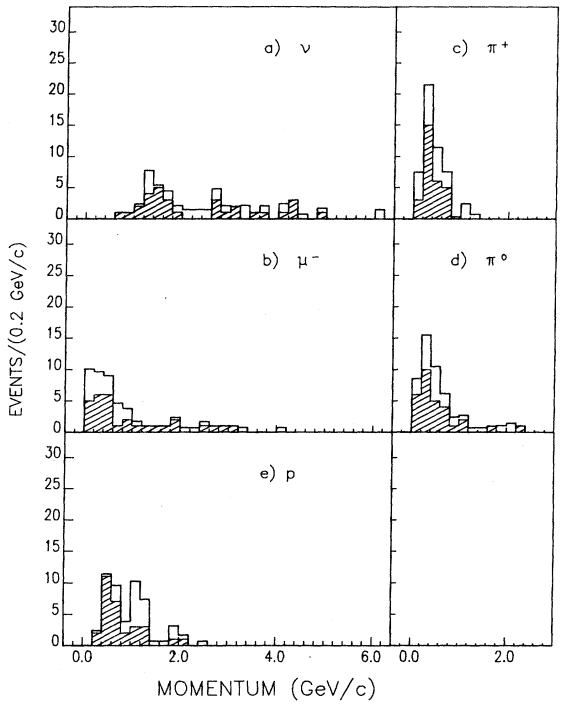

FIG. 4. Momentum distributions for reaction (2). The cross-hatched areas are the uniquely chosen events for the reaction. The blank areas are the ambiguous events weighted as discussed in the text.

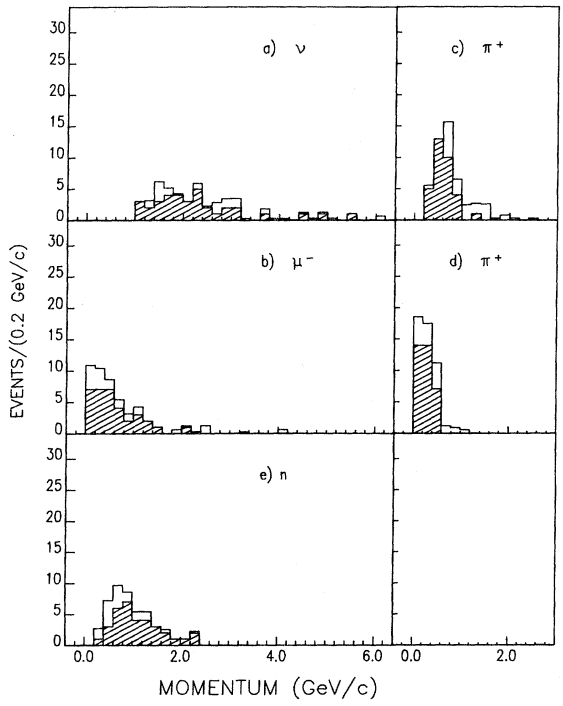

FIG. 5. Momentum distributions for reaction (3). The cross-hatched areas are the uniquely chosen events for the reaction. The blank areas are the ambiguous events weighted as discussed in the text.

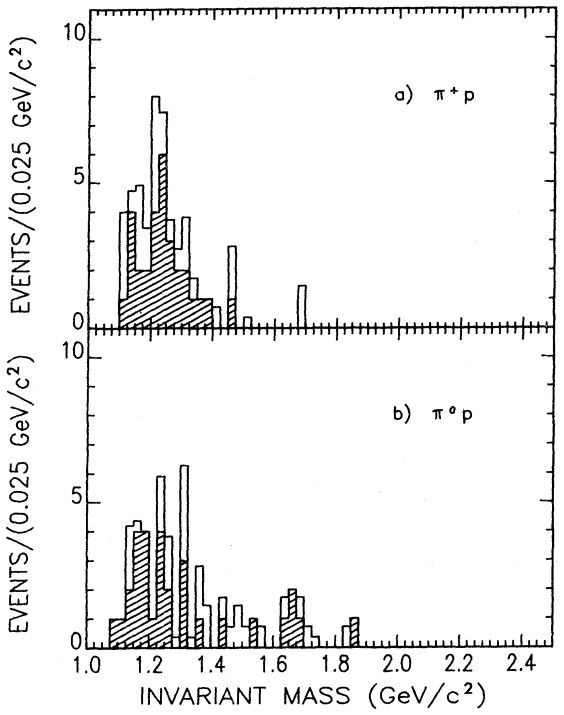

FIG. 6. Invariant-mass distributions for reaction (2) involving one pion with the proton. The cross-hatched areas are the uniquely chosen events for the reaction. The blank areas are the ambiguous events weighted as discussed in the text.

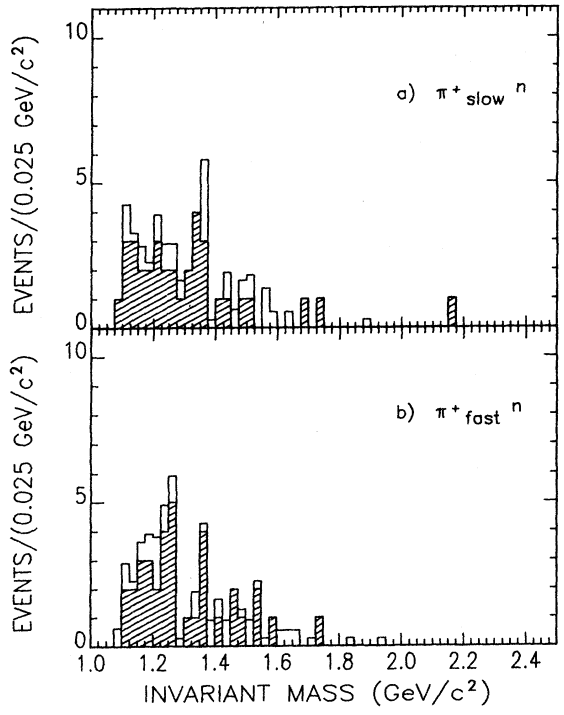

FIG. 7. Invariant-mass distributions for reaction (3) involving one pion with the neutron. The cross-hatched areas are the uniquely chosen events for the reaction. The blank areas are the ambiguous events weighted as discussed in the text.

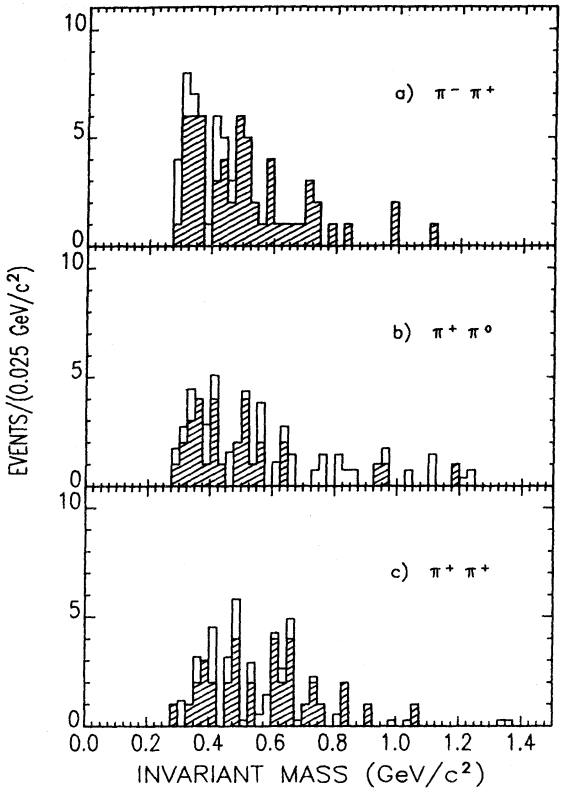

FIG. 8. Invariant-mass distributions for the three reactions for the two-pion system. The cross-hatched areas are unique events. For (a) the blank areas are events with $M(\pi^- p) = M(\Lambda) \pm 15$ MeV/c^2, while in (b) and (c) the blank areas are the ambiguous events weighted as discussed in the text.

tions $\nu d \to \mu^- p p_s$ and $\nu d \to \mu^- \pi^+ p n_s$ with χ^2 probability greater than 1% and also events giving a 0C solution to the reactions $\nu d \to \mu^- \pi^0 p p_s$ or $\nu d \to \mu^- \pi^+ n p_s$ with spectator proton momentum less than 350 MeV/c. In addition, events that gave an acceptable 1C kinematic fit to the neutron background reaction $nd \to \pi^- p p n_s$ with χ^2 probability greater than 5% were also removed.[8]

An additional cut is necessary for reaction (3) because a large number of charged hadrons enter from the sides of the bubble chamber, scatter, and produce spurious fits. Such bogus fits tend to have outgoing neutrons with high momentum and small angle $\theta_{\nu N}$ with respect to the neutrino-beam direction. This effect can be investigated by comparing the $\theta_{\nu N}$ distribution of reaction (3) with that of the other two reactions (see Fig. 3). Assuming that the kinematics for the struck nucleon in the three reactions are similar, one expects all three distributions to be similar for the genuine events. This expectation is reasonably well fulfilled for (1) and (2). However, for reaction (3) a large excess of events with $\theta_{\nu N} < 10^\circ$ occurs, representing the spurious fits. Therefore, only events with $\theta_{\nu N} > 10^\circ$ were retained. The loss of genuine events due to this cut is estimated to be $10 \pm 7\%$ (see Table I) and was obtained from the distribution of the other two reactions.

As before, in order to be called a muon the negative

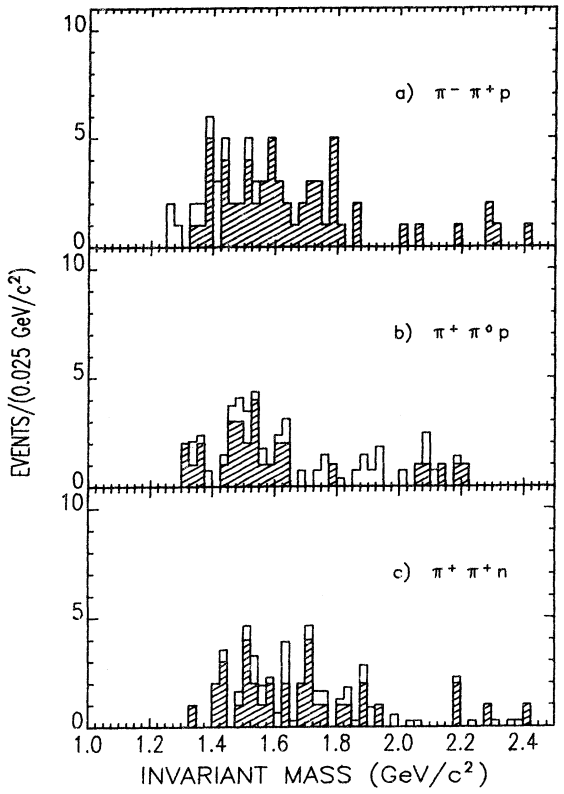

FIG. 9. Invariant-mass distributions for the three reactions for the total hadronic system. The cross-hatched areas are unique events. For (a) the blank areas are events with $M(\pi^-p)=M(\Lambda)\pm15$ MeV/c^2, while in (b) and (c) the blank areas are the ambiguous events weighted as discussed in the text.

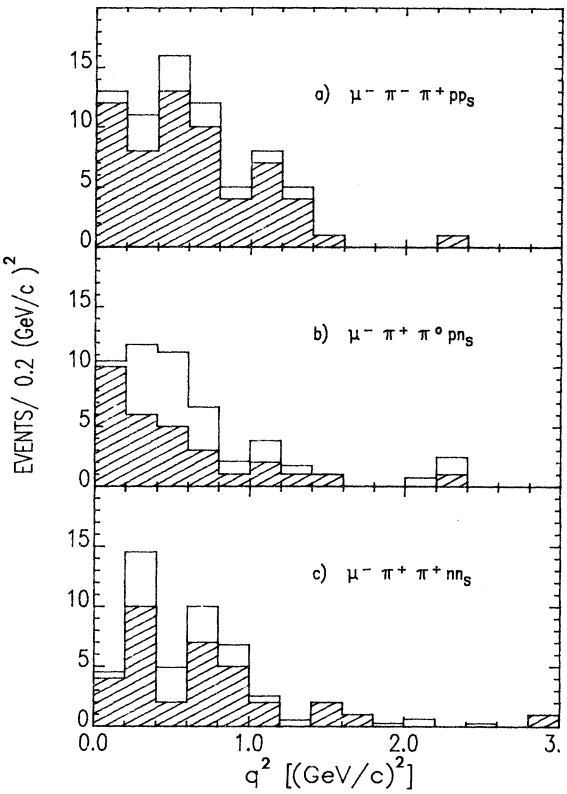

FIG. 10. Distributions for the four-momentum transfer squared for the three reactions. The cross-hatched areas are unique events. For (a) the blank areas are events with $M(\pi^-p)=M(\Lambda)\pm15$ MeV/c^2, while in (b) and (c) the blank areas are the ambiguous events weighted as discussed in the text.

track had to either leave the chamber without interacting or decay into an electron. In addition, visual information was used wherever possible to resolve ambiguities.

The final data sample then consists of 30 events unique to reaction (2), 35 events unique to reaction (3), and 37 events ambiguous between the two reactions, essentially because the π^+/proton track ambiguity could not be resolved. The distribution of the proton momentum for unique events of reaction (2) together with that of the fast π^+ for unique events of reaction (3) are given in Table II.[9] Assuming that, in any given momentum interval, the ambiguous sample contains the same ratio of protons to pions as does the unique sample, we estimate that 22 events belong to reaction (2) and 15 events to reaction (3), with an estimated uncertainty of ±5 events. We would then have 52 and 50 events, respectively, for reactions (2) and (3). The laboratory momentum distributions for each of the particles in reactions (2) and (3) are presented in Figs. 4 and 5, respectively. These distributions are very similar to those of reaction (1) shown in Fig. 1.

III. EXPERIMENTAL RESULTS

A. General properties of the reactions

The pion-nucleon invariant-mass distributions for reactions (1), (2), and (3) are shown in Figs. 2, 6, and 7. These distributions are all characterized by the presence of low-mass enhancements involving $\Delta(1236)$ production.

The $\pi\pi$ invariant-mass distributions for the three reactions are shown in Fig. 8. There is no clear evidence for the production of any known resonances in these distributions. At our energies, diffractive ρ production is expected to be strongly kinematically suppressed. Based upon the prediction of Chen *et al.*,[10] one expects the number of ρ^0 and ρ^+ to be 10^{-3} of the total number of νn and νp in-

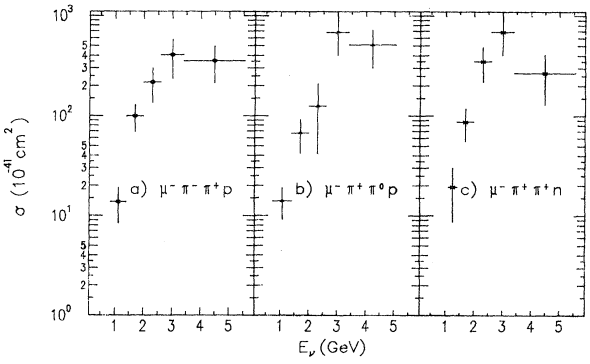

FIG. 11. The excitation functions for the three reactions.

TABLE III. Cross sections.

E_ν (GeV)	ΔE_ν (GeV)	No. of events	σ (10^{-41} cm^2)
		Reaction (1)	
1.125	0.275	9.5	13.7±5.3
1.700	0.300	20.0	99.0±30.0
2.300	0.300	9.0	216±81
3.000	0.400	7.0	404±168
4.475	1.075	8.0	352±140
		Reaction (2)	
1.075	0.325	9.0	14.0±4.8
1.700	0.300	9.5	66.7±24.6
2.300	0.300	3.6	125±83
3.000	0.400	8.3	681±276
4.225	0.825	9.0	511±209
		Reaction (3)	
1.250	0.150	3.5	19.3±10.6
1.700	0.300	11.1	87.0±31.1
2.300	0.300	9.2	350±131
3.000	0.400	7.5	690±286
4.475	1.075	4.3	267±137

teractions, respectively. For our sample[5,6] this corresponds to two ρ^0 and one ρ^+, consistent with the absence of an observed signal.

The $N\pi\pi$ invariant-mass distributions for reactions (1)—(3) are shown in Fig. 9. There is no clear evidence for resonance production in any of these final states.

The distributions in four-momentum transfer squared (q^2) are shown in Fig. 10. The resolution in q^2 is smaller than the binning. There is clearly a bias against events with low q^2 where the struck nucleon would be difficult to detect. A similar bias has been observed in a study of the reaction $\pi^- n \to \pi^- \pi^- p$ where events with low q^2 impart so little momentum to the struck nucleon that the resultant nucleon goes unnoticed.[11] An estimate of our losses due to this effect is given in Table I.

B. Excitation functions for the reactions

The momentum spectrum of neutrinos which interact via reactions (1)—(3) [Figs. 1(a), 4(a), and 5(a), respectively] peak at an energy of ~1.5 GeV, in contrast to the case of single-pion production where the peak occurs at 0.9 GeV.[5] The cross sections for reactions (1)—(3) as a function of ν energy are shown in Fig. 11 and listed in Table III. The error bars on the cross sections contain both the overall normalization uncertainty of ±15% and a point-to-point relative error in the flux shape of ±5% folded in, except for the last point for each reaction where we use ±15% to allow for the uncertainty in the parent K^+ flux from which the higher-energy neutrinos come. All of the cross sections rise rapidly from threshold and appear to peak at $E_\nu \sim 3$ GeV. The behavior above 3 GeV cannot be determined on the basis of only one measured data point, but it does appear that the rapid rise from threshold is not sustained. This behavior is similar to that shown by the quasielastic scattering reaction and by the two-body processes involving N^* and Δ production.[1,3,5,6]

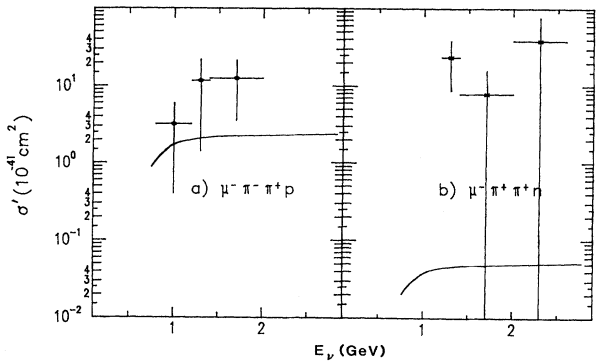

FIG. 12. Total cross sections for the restricted phase space specified by Adjei, Dicus, and Teplitz. The curves are the theoretical predictions where $\xi=0$ and $\eta=\frac{3}{4}$.

A model of weak dipion production close to threshold has been recently studied by Adjei, Dicus, and Teplitz,[12] who were motivated by the possibility of determining the chiral-symmetry-breaking parameter ξ, previously measured from strong two-pion production in $\pi N \to \pi\pi N$. This parameter is important in estimating the strong final-state $\pi\pi N$ interactions in weak dipion production. Following Adjei, Dicus, and Teplitz, we compare our data to the model prediction for the largest of the phase-space intervals considered ($\eta=\frac{3}{4}$). For each of the reactions we extracted the threshold cross section σ' for the production of events with energy less than ηm_π above threshold in the $\pi\pi$ and $\pi\pi N$ center-of-mass systems. The number of such threshold events in our full data sample is 10, 0, and 4 for reactions (1), (2), and (3), respectively.[12] Our results are presented in Fig. 12 along with the predictions of Adjei, Dicus, and Teplitz. While the agreement is good for reaction (1), it is less so for reaction (3). Adjei, Dicus, and Teplitz also predict that the threshold cross section σ' for reaction (3) should be twice that for reaction (2), while the number of observed events are 4 and 0, respectively. For reactions (1) and (3) the average values of σ', over the observed E_ν intervals, are $(6.5\pm3.1)\times10^{-41}$ cm^2 and $(17\pm9)\times10^{-41}$ cm^2, respectively.

C. Test of the conserved-vector-current hypothesis

The Adler[13] test of the conserved-vector-current (CVC) hypothesis can be directly applied to our data. For CVC to be valid, the expectation value of the pseudoscalar triple product

$$\bar{\psi} \equiv \langle \vec{\mu}^- \cdot (\vec{\pi}^- \times \vec{\pi}^+) \rangle \tag{4}$$

must be zero as the angle $\theta_{\nu\mu}$ between the μ^- and ν directions approaches zero. In the expression for the triple product, the vectors represent the momentum vectors for the respective particles in the laboratory system.

The CVC test was applied only to the relatively clean sample of 3C fits belonging to reaction (1). Approximate-

TABLE IV. Mean triple products.

$\theta_{\nu\mu}$ (degrees)	$\bar{\psi}$	$\sigma_{\bar{x}}$	No. of events
0.00–22.50	0.002	0.082	7
22.50–45.00	−0.018	0.015	11
45.00–67.50	−0.003	0.010	11
67.50–106.6	−0.003	0.003	9

ly 48% of these events have a μ^-/π^- ambiguity. Since the triple product is antisymmetric under the interchange of μ^- and π^-, these ambiguous events are expected to yield an average value of zero for the triple product, quite independent of any CVC expectations, and an average value of zero is indeed observed for this data sample. It is therefore important to remove these ambiguous events before checking CVC. These μ^-/π^- ambiguities arise primarily from the fact that the location of the interaction in the fiducial volume is such that the path lengths of the negative tracks in the bubble chamber are too short to permit identification of at least one of the tracks. Since the ambiguity is geometrical in origin, the exclusion of ambiguous events does not constitute a bias.

The results are shown in Table IV and Fig. 13. The probability that the average value of the triple product is zero over all events is greater than 66%, and is almost 100% for the first bin which contains events with the smallest values of $\theta_{\nu\mu}$. We therefore conclude that the data are consistent with the CVC hypothesis.

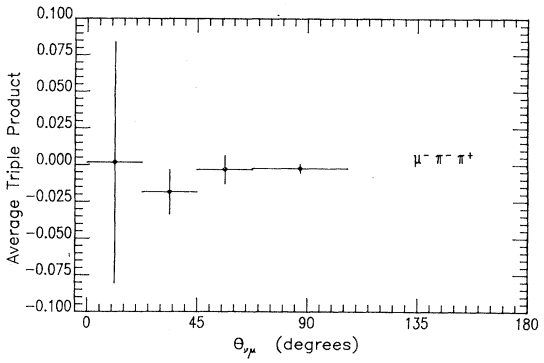

FIG. 13. Plot of the triple-product test of CVC for reaction (1).

ACKNOWLEDGMENTS

We would like to thank the 12-foot bubble-chamber crew and our scanning and measuring staffs for their help. This work was supported by the U.S. Department of Energy and the National Science Foundation. We would also like to thank D. McKay and A. Actor for useful discussions.

[a] Present address: U. S. Department of Energy, Washington, D.C. 20545.
[b] Present address: Gulf Oil Corp., Harmerville, PA 15204.
[c] Present address: University of Toronto, Toronto, Ont., Canada.
[d] Present address: Los Alamos National Laboratory, Los Alamos, NM 87545.
[e] Present address: University of Colorado, Boulder, CO 80309.
[f] Present address: Bell Telephone Laboratories, Naperville, IL 60540.
[g] Present address: Louisiana State University, Baton Rouge, LA 70803.
[h] Present address: Valparaiso University, Valparaiso, IN 46383.
[i] Present address: Rutgers University, New Brunswick, NJ 08903.
[j] Present address: Technion, Haifa, Israel.
[k] Present address: Center for Naval Analyses, Alexandria, VA 22311.

[1] S. J. Barish *et al.*, Phys. Rev. D 16, 3103 (1977).
[2] S. Bonetti *et al.*, Nuovo Cimento 38, 260 (1977).
[3] S. J. Barish *et al.*, Phys. Rev. D 19, 2521 (1979).
[4] J. Bell *et al.*, Phys. Rev. Lett. 41, 1008 (1978); 41, 1012 (1978).
[5] G. M. Radecky, Ph.D. thesis, Purdue University, 1980; G. M. Radecky *et al.*, Phys. Rev. D 25, 1161 (1982).
[6] K. L. Miller *et al.*, Phys. Rev. D 26, 537 (1982).
[7] J. Bell *et al.*, Phys. Rev. Lett. 40, 1226 (1978).
[8] For a discussion of the neutron background in this experiment, see M. Derrick *et al.*, Phys. Lett. 92B, 363 (1980).
[9] A similar technique was used to make mass assignments in the 0C single-pion-production events (see Ref. 5).
[10] M.-S. Chen *et al.*, Nucl. Phys. B118, 345 (1977).
[11] D. Cohen *et al.*, Phys. Rev. D 7, 661 (1973).
[12] S. A. Adjei, D. A. Dicus, and V. L. Teplitz, Phys. Rev. D 24, 623 (1981). The data used by these authors were based on our preliminary results and are superseded by the data now presented.
[13] S. L. Adler, Phys. Rev. B135, 963 (1964).